Remodeling of the Bacterial RNA Polymerase Supramolecular Complex in Response to Environmental Conditions†

Seema Verma, Yijia Xiong, M. Uljana Mayer, and Thomas C. Squier*

Cell Biology and Biochemistry Group, Biological Sciences Division, Pacific Northwest National Laboratory, Richland, Washington 99352

Received October 10, 2006; Revised Manuscript Received January 4, 2007

ABSTRACT: Directed binding of RNA polymerase to distinct promoter elements controls transcription and promotes adaptive responses to changing environmental conditions. To identify proteins that modulate transcription, we have expressed a tagged α-subunit of RNA polymerase in *Shewanella oneidensis* under controlled growth conditions, isolated the protein complex using newly developed multiuse affinity probes, and used LC−MS/MS to identify proteins in the complex. Complementary fluorescence correlation spectroscopy measurements were used to determine the average size of the RNA polymerase complex in cellular lysates. We find that RNA polymerase exists as a large supramolecular complex with an apparent mass in excess of 1.4 MDa, whose protein composition substantially changes in response to growth conditions. Enzymes that copurify with RNA polymerase include those associated with tRNA processing, nucleotide metabolism, and energy biosynthesis, which we propose to be necessary for optimal transcriptional rates.

Shewanella oneidensis MR-1 is a facultatively anaerobic Gram-negative bacterium that possesses one of the more versatile respiration capabilities demonstrated to date by a single microorganism (*1*). Under optimal growth conditions, approximately 80% of DNA-directed RNA polymerase (RNAP)[1] complexes are bound to operons encoding the synthesis of stable RNA (i.e., tRNA and rRNA), which comprise approximately 1% of the genome and whose biosynthesis limits cell growth under optimal conditions (*2*−*4*). Under poor growth conditions, there are rapid shifts in gene transcription that result in a large increase in the diversity of gene expression and corresponding decreases in stable RNA production (*2*, *5*−*7*). Underlying these adaptive shifts in metabolism is the regulation of the association between the RNAP multiprotein enzyme complex and specific promoter elements on DNA, which occurs in response to the recruitment of transcription factors and other proteins that associate with the RNA polymerase core ($\alpha_2\beta\beta'$) (*8*, *9*).

Transcriptional regulators (e.g., CRP or NusA) either enhance or weaken binding of RNAP to specific promoters to modulate rates of both elongation and termination (*8*, *9*). Indeed, both CRP and NusA are known to recruit RNAP to relevant promoter sites through direct binding to the α-subunit of the polymerase. Further, bacterial cells contain multiple forms of the RNAP complex, the composition of which changes in response to environmental conditions (*10*). These prior observations, coupled with recent suggestions that between 22 and 49 proteins are copurified with the α-subunit of RNAP (*11*), suggest a need to quantitatively assess the range of protein associations between transcriptional regulatory proteins and RNAP.

With the aim of understanding the link between environmental conditions and possible changes in the size and composition of the RNAP complex that contribute to cellular function, we have grown *S. oneidensis* under controlled growth conditions using a bioreactor in which lactate was used as a carbon source under aerobic (i.e., 20% oxygen) or suboxic conditions (i.e., 0.1% oxygen) (see Figure S1 of the Supporting Information), which have previously been shown to result in both dramatic metabolic shifts and large changes in protein abundances (*6*, *12*). The use of bioreactors permits real-time measurements of growth conditions that allow an experimental consideration of how environmental changes induce alterations in protein abundances and prevents common artifacts associated with shaker flasks in which bacterial metabolism can dramatically affect substrate and oxygen concentrations. We have focused on the molecular regulation involving the α-subunit of RNAP, which directly binds to promoter regions to mediate transcriptional activation and is regulated through binding interactions with a range of

† This work was supported by the Genomics:GTL Program of the U.S. Department of Energy Office (DOE) of Biological and Environmental Research. Battelle is operated for DOE under Contract DE-AC05-76RL0 1830.

* To whom correspondence should be addressed: Cell Biology and Biochemistry Group, 790 6th St., Mail Stop P7-53, Pacific Northwest National Laboratory, Richland, WA 99354. Telephone: (509) 376-2218. Fax: (509) 376-6767. E-mail: thomas.squier@pnl.gov.

[1] Abbreviations: β-ME, 2-mercaptoethanol; CaM, calmodulin; CrAsH, carboxyl-FlAsH; DMPS, 2,3-dimercaptoproylsulfonate; DTT, dithiothreitol; EDC, 1-[3-(dimethylamino)propyl]-3-ethylcarbodiimide; EDT, ethanedithiol; ESI-MS, electrospray ionization mass spectrometery; FCS, fluorescence correlation spectroscopy; FlAsH-EDT_2, 4′,5′-bis-(1,3,2-dithioarsolan-2-yl)fluorescein(1,2-ethanedithiol)$_2$; HEPES, *N*-(2-hydroxyethyl)piperazine-*N*′-2-ethanesulfonic acid; MAP, multiuse affinity probe; MS, mass spectrometry; NTA, nitrilo triacetic acid; PIPES, piperazine-1,4-bis(2-ethanesulfonic acid); RNAP, DNA-dependent RNA polymerase; SDS−PAGE, sodium dodecyl sulfate−polyacrylamide gel electrophoresis; TCEP, tris(carboxyethyl)phosphine; TLC, thin-layer chromatography.

10.1021/bi0621157 CCC: $37.00
Published on Web 02/24/2007

transcriptional activators, including members of the CRP and AraC/XylS families. Estimates of the size of the RNAP complex and its subsequent affinity isolation were made through the molecular tagging of the α-subunit of RNAP with a tetracysteine-binding motif, which binds multiuse affinity probes (MAPs) with high affinity (i.e., $K_d = 10$ pM) (*13*). Multiuse affinity probes (MAPs) immobilized on glass beads permit a one-step isolation of the RNAP complex using mild elution conditions and retention of the macromolecular complex (*11*). Our results demonstrate that RNAP is a large multiprotein complex with a mass in excess of 1.4 MDa, the subunit composition of which indicates an increased translational efficiency associated with the synthesis of stable RNA under aerobic conditions and the subunit composition of which is substantially remodeled under suboxic conditions.

EXPERIMENTAL PROCEDURES

Chemicals and Materials. Acetonitrile was purchased from Aldrich Chemical Co. (Milwaukee, WI). Ammonium bicarbonate and methanol were obtained from Fisher Scientific (Fair Lawn, NJ). Sequencing grade, modified trypsin was purchased from Promega (Madison, WI). Complete EDTA-free protease inhibitor cocktail tablets (catalog no. 1873580) were from Roche (Indianapolis, IN). The Bradford reagent was from Bio-Rad (Hercules, CA). Ni-NTA Superflow Agarose was purchased from Qiagen (Valencia, CA). TCEP was purchased from Pierce (Rockford, IL). Urea, DTT, 2,3-dimercaptoproylsulfonate (DMPS), $CaCl_2$, and other reagents were obtained from Sigma-Aldrich (St. Louis, MO). Antibodies against the α- and β-subunits of RNAP from *Escherichia coli* were from Neoclone (Madison, WI). All chemicals used for the affinity resin synthesis were obtained from Aldrich, except for the glass beads, which are from Prime Synthesis (Aston, PA).

Synthesis of Affinity Resin (FlAsH-derivatized glass beads). Carboxy-FlAsH (i.e., CrAsH) was synthesized as previously described (*14*). CrAsH (1.43 g, 0.0015 mol, 1 equiv) was dissolved in dry dimethyl sulfoxide. 1-[3-(Dimethylamino)-propyl]-3-ethylcarbodiimide (EDC) (0.6 g, 2 equiv) and *N*-hydroxysuccinimide (0.17 g, 1 equiv) were added, and the reaction was monitored by TLC in a 20% methanol/ethyl acetate mixture. A new spot appeared at 5 min, and the reaction was close to completion at 20 min. At this time, 20 g of aminopropyl glass resin (Prime Synthesis) was added, as well as 100 μL of triethylamine. The reaction was allowed to proceed overnight. Subsequently, the resin was washed three times each with DMSO, ethyl acetate, DMSO, water, and phosphate buffer (pH 7.0) and finally stored in phosphate buffer and 20% ethanol.

Cloning and Expression of the α-Subunit of RNA Polymerase and Cell Cultivation. A C-terminal 52-amino acid sequence was appended onto the α-subunit of RNA polymerase (SO0256) cloned into the pBAD202/D-TOPO vector (Invitrogen) containing in the following order a tetracysteine tag (AREACCPGCCK) adjacent to a V5 epitope (KGGRADPAFLYKVVINSKLEGKPIPNPLLGL) and a His_6 sequence at the C-terminus, as previously described (*11*). The pBAD/D-TOPO expression system contains the promoter of the *araBAD* (arabinose) operon, which can be upregulated by arabinose and downregulated by glucose to permit optimal expression. Plasmids were maintained by addition of 20 μg/mL kanamycin. Following transformation of *S. oneidensis* either with the pBAD/D-TOPO vector alone or following the insertion of the α-subunit of RNA polymerase, cells were grown in a 14 L BioFlo 3000 bioreactor (New Brunswick Inc., Edison, NJ), permitting continuous monitoring of culture conditions under either aerobic (i.e., 20% dissolved oxygen tension) or suboxic (i.e., 0.1% dissolved oxygen tension) conditions with DL-lactate as a carbon source, essentially as previously described (see Figure S1 of the Supporting Information) (*12*, *15*, *16*). Briefly, reactors were maintained at 30 °C and neutrality (i.e., pH 7.0) with continuous addition of fresh media to the reactor at a rate of 9 mL/min under either aerobic or suboxic conditions, which involved agitation at either 450 (aerobic) or 50 rpm (suboxic) and addition of 100% air, resulting in a steady-state optical density of either 1.5 (aerobic) or 0.5 (suboxic). Media contained the following: 3 mM PIPES, 1.8 mM NaH_2PO_4, 90 mM DL-lactate, 1.3 mM KCl, 5.6 mM NH_4Cl, 1 μM Na_2SeO_4, and 80 μM ferric NTA in addition to the minerals 0.2 μM $AlK(SO_4)_2$, 2 μM H_3BO_3, 7 μM $CaCl_2$, 4 μM $CoCl_2$, 0.4 μM $CuSO_4$, 4 μM $FeSO_4$, 30 μM $MnSO_4$, 0.2 mM NaCl, 1 μM Na_2MoO_4, 0.25 mM $MgSO_4$, 1 μM Na_2WO_4, 1 μM $NiCl_2$, and 10 μM $ZnCl_2$, vitamins (80 nM biotin, 40 nM folic acid, 0.6 μM pyridoxine, 0.13 μM riboflavin, 0.15 μM thiamine, 0.4 μM nicotinic acid, 0.2 μM pantothenic acid, 0.6 nM B-12, 40 nM *p*-aminobenzoic acid, and 0.24 μM lipoic acid), and amino acids (0.13 mM L-Arg, 0.16 mM L-Glu, and 0.23 mM D/L-Ser). Cells were pumped from the fermentor, pelleted, resuspended in buffer A [50 mM HEPES (pH 7.5), 150 mM NaCl, and 10 mM TCEP], transferred to 5 mL cryotubes in 2 g (wet weight) aliquots, quick-frozen in liquid nitrogen, and stored at −80 °C for further analysis.

Cell Lysis. Frozen cell suspensions were thawed, and lysate-containing protease inhibitor cocktail [1 tablet per 10 mL (catalog no. 1873580; Roche)] was prepared by probe sonication (model 100 sonic dismembrator, Fisher Scientific, Pittsburgh, PA) in an ice bath for 6 × 1 min, at output 11 with an interval of 1 min each, and then centrifuged at 17200*g* for 25 min to remove cell debris. The lysis buffer contained 25 mM HEPES (pH 7.6), 0.3 M NaCl, 10 mM imidazole, and 2 mM β-ME. The cleared supernatant was subjected to a Bradford assay (Bio-Rad) to determine the protein content of the lysate.

Isolation of the RNAP Protein Complex. Prior to incubation with cellular lysates, 60 μL of FlAsH-derivatized glass beads was washed once with buffer A [50 mM HEPES, 150 mM NaCl (pH 7.5), 10 mM TCEP] and 10 mM ethanedithiol (EDT) and then twice with buffer A alone. Washed beads were then incubated with 5.0 mL of lysate (8 mg/mL) expressing either the α-subunit of RNAP or an empty vector control and rotated overnight on a shaker at 4 °C. The next day, beads were washed once with the buffer A and then with buffer B [100 mM ammonium bicarbonate (pH 7.5) containing 5 mM TCEP]. During washes, the protein content was monitored using the Bradford assay and a final wash to release remaining nonspecific associations involving buffer B containing 5 mM β-ME. After the final wash, beads were transferred to fresh tubes and proteins bound to the resin were eluted using 0.2 mL of buffer C [100 mM ammonium bicarbonate (pH 7.5), 5 mM β-ME, and 50 mM 2,3-dimercaptoproylsulfonate (DMPS)] at 4 °C with a final yield

of approximately 40 μg of total protein.

Alternatively, RNAP complexes were isolated using the His_6 tag with Ni-NTA agarose beads from Qiagen. Briefly, 30 mL of cellular lysate (12 mg/mL) overexpressing the α-subunit of RNAP was incubated with 3 mL of Ni-NTA beads overnight on a shaker at 4 °C. The next day, nonspecific proteins were removed through extensive washing first with 20 column volumes of lysis buffer and then 50 column volumes of wash buffer [25 mM HEPES (pH 7.6), 0.5 M NaCl, 40 mM imidazole, and 2 mM β-ME]. Finally, the RNAP complex was eluted in 25 mM HEPES (pH 7.6), 0.5 M NaCl, 0.4 M imidazole, and 2 mM β-ME. The amount of protein eluted was measured by a Bradford assay to be approximately 2 mg of total protein.

Trypsin Digestion. Prior to LC−MS/MS analysis, isolated protein complexes were denatured (7 M urea and 5 mM DTT for 30 min at 60 °C) before addition of sequencing grade modified trypsin (Promega) (2% by weight ratio of total protein) for 5 h at 37 °C in the presence of 100 mM ammonium bicarbonate (pH 8.4), essentially as previously described (*12*). Samples were desalted using a SPE C18 column (1 mL) (Supelco-Sigma, St. Louis, MO) preequilibrated with methanol, rinsed with 2 mL of nanopure H_2O, and washed with 2 mL of a 95% water/5% acetonitrile mixture. Proteins were then eluted using a 70% acetonitrile/30% H_2O mixture followed by a 90% acetonitrile/10% H_2O mixture and then concentrated using a SpeedVac. Protein concentrations were measured using the bicinchoninic acid (BCA) protein assay (Pierce).

LC−MS/MS Acquisition. Tryptic digests were each analyzed in triplicate (technical replicates) using a fully automated custom-built capillary HPLC system coupled online with an LTQ ion trap mass spectrometer (ThermoFinnigan, San Jose, CA) using an in-house manufactured electrospray ionization interface, as described previously (*12*). The reversed phase capillary column was slurry packed using 3 μm Jupiter C_{18} particles (Phenomenex, Torrence, CA) into a 150 μm (inside diameter) × 65 cm fused silica capillary (Polymicro Technologies, Phoenix, AZ). The mobile phases consisted of 0.2% acetic acid and 0.05% TFA in water (phase A) and 0.1% TFA in 90% acetonitrile (phase B). An exponential gradient was employed in the separation, which started with 100% A and gradually increased to 60% B over 100 min. The instrument was operated in data-dependent mode with an *m*/*z* range of 400−2000. The five most abundant ions from MS analysis were selected for further MS/MS analysis using a normalized collision energy setting of 35%. To avoid repetitive analysis of the same abundant precursor ion, 1 min dynamic exclusion was used.

MS/MS Data Analysis. MS/MS data were searched against the *Shewanella*_2003−12-19.fasta database (*17*) and a sequence-reversed IPI database (to assess false positives) using SEQUEST (ThermoFinnigan). All data files were extracted using Prism Data Extractor version 1.2.7 (http://ncrcpnl.gov/about/process.stm) and exported to Access (Microsoft Inc., Redmond, WA). Two different filtering criteria were used to identify peptides from the raw SEQUEST data: (1) using a simple criterion requiring that X_{corr} be ≥2.6 for full tryptic peptides, X_{corr} be ≥2.8 for partially tryptic peptides, and the sp score be ≥500 (*18*) and (2) requiring that X_{corr} be ≥1.6 for the +1 charge-state full tryptic peptides, ≥2.4 for the +2 charge-state full tryptic peptides, ≥4.3 for partial tryptic peptides, ≥3.2 for the +3 charge-state full tryptic peptides, and ≥4.7 for partial tryptic peptides for which $\Delta C_n > 0.1$ (*19*). Using these criteria, we were able to identify 360 proteins using the first filter and 441 proteins using the second filter that copurified with RNAP, where there were 3.3 and 0.0% false-positive identifications, respectively, based on the reversed database. For greater confidence, we only considered the 341 proteins confidently identified using both filters for further analysis. Of the identified proteins, 95% of the identified peptides contained fully tryptic cleavage sites. The sum of X_{corr} (i.e., $\sum X_{corr}$) for all peptides passing the SEQUEST criteria was calculated for each of three independent biological replicates, which were measured in triplicate for both samples expressing the α-subunit of RNAP (nine measurements) and empty vector controls (nine measurements). Subsequently, a normalized $\sum X_{corr}$ value (i.e., $\langle X_{corr} \rangle$) was calculated for each of the 18 measurements, where

$$\langle X_{corr} \rangle = \sum X_{corr_i} / \sum_{i=1}^{n} \sum X_{corr_i} / n \quad (1)$$

Relative abundance changes between samples expressing the α-subunit of RNAP and empty vector controls were visualized using hierarchical clustering settings in Omniviz 3.6.1 (www.omniviz.com). Alternatively, for those proteins that had at least one peptide which passed the SEQUEST criteria in each of three biological replicates involving the independent affinity isolation of the RNAP complex, changes in the relative abundance of proteins isolated in association with the α-subunit of RNAP relative to empty vector controls were calculated

$$\text{abundance} = \sum_{i=1}^{9} \sum X_{corr_i} (\alpha\text{-subunit RNAP}) / \sum_{i=1}^{9} \sum X_{corr_i} (\text{empty vector control}) \quad (2)$$

Fluorescent Labeling. The α-subunit of RNAP or calmodulin (CaM) was covalently labeled using the Alexa-488 protein labeling kit from Molecular Probes. Briefly, either the α-subunit of RNAP or CaM (1.0 mg) in 0.5 mL of 0.1 M Na_2CO_3 (pH 8.3) was incubated with Alexa-488 for 1 h at 20 °C, and unbound dye was removed using a G-25 Sephadex column. Stoichiometries of dye binding were determined by measuring the absorbance at 495 nm, where ϵ_{494}(Alexa-488) = 71 000 M^{-1} cm^{-1} (*20*). In all cases, an equimolar amount of bound dye was associated with the labeled protein.

Fluorescence Correlation Spectroscopy. The α-subunit of RNAP labeled with Alexa-488 (5 nM) was equilibrated for approximately 1 h with cellular lysate prior to all measurements. Fluorescence correlation spectra were obtained using a Nikon TE300 inverted microscope modified for these measurements. The excitation laser was a Coherent Innova400 model (488 nm) focused by a 100× objective lens (S Fluo100, Nikon), which was focused 50 μm above the surface of the cover glass. Data were recorded for approximately 5 min with an excitation laser power of 45 μW measured at the entry port of the microscope. The fluorescence was collected using the same objective, separated by a 505DCLP dichroic mirror (Chroma Technologies, Brattle-

boro, VT), split by a cube beam splitter (Thorlabs, Newton, NJ), and then collected subsequent to HQ535 emission filters (Chroma Technologies). The resulting fluorescence was detected by a pair of SPCM-AQR-14 avalanche photodiodes (Perkin-Elmer Optoelectronics, Vaudreuil, QC). The output was detected by a Flex01-05D multi-tau correlator (Correlator.com, Bridgewater, NJ). The curves were analyzed using the following "Triplet-State" model by nonlinear fitting function in the program Origin (MicroCal, Northampton, MA):

$$G(t) = 1 + \left(1 + \frac{f_T}{1 - f_T} e^{-t/\tau_T}\right)\frac{1}{N}\frac{1}{1 + \frac{t}{\tau_D}\sqrt{1 + S^2\frac{t}{\tau_D}}} \quad (3)$$

where t is the lag time between two channels, f_T and τ_T are the fractional population and decay time of the triplet state, respectively, and N is the total number of fluorescent molecules within the focus point. S is a structural parameter of the experimental setup assumed to be 5. τ_D is the diffusion time of the molecule. The relation between the diffusion time and translational diffusion coefficient (D_t) is

$$D_t = \frac{\omega^2}{4\tau_D} \quad (4)$$

where ω is the lateral radius of the focus volume. The Stokes−Einstein formula can be used to estimate the hydrodynamic radius (R) of the complex assuming a spherical particle:

$$R = \frac{kT}{6\pi\eta D_t} \quad (5)$$

where k is the Boltzmann constant (1.38×10^{-23} J/K), T is the absolute temperature, (293 K), and η is the viscosity of water (0.89 cP). From the hydrodynamic radius of the molecule, the molecular mass (m) can be calculated.

$$m = 4\pi\rho N_A R^3/3 \quad (6)$$

where N_A is Avogadro's number and ρ is the mean density of the molecule.

RESULTS

Increased Abundance of RNAP under Aerobic Growth Conditions. Possible abundance changes in RNAP in response to environmental growth conditions were assessed by comparing the concentrations of the α- and β-subunits of RNAP under aerobic and suboxic conditions using cells transformed with the pBAD/D-TOPO empty vector. Using antibodies raised against the homologous subunits of RNAP in *E. coli*, we observe single bands corresponding to either the α- or β-subunit in lysates from *Shewanella* grown under both aerobic and suboxic conditions, with apparent molecular masses of 36.6 and 150 kDa (Figure 1). Comparison with authentic protein standards suggests that the α- or β-subunit of RNAP each comprise ~0.3% of the expressed protein in lysates, consistent with earlier estimates that under aerobic conditions RNAP comprises approximately 1% of the total protein (*21*). In comparison, under suboxic conditions, there

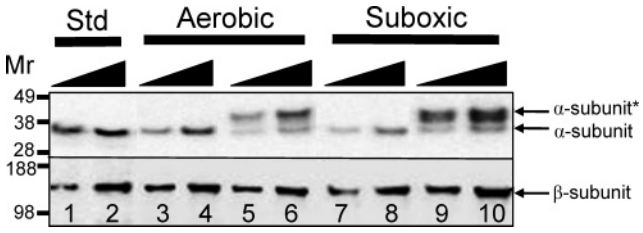

FIGURE 1: Increased abundances of α- and β-subunits of RNAP under aerobic conditions (20% oxygen tension) in comparison to suboxic (0.1% oxygen tension) growth conditions for empty vector controls (lanes 3, 4, 7, and 8) and changes in protein abundances following expression of a tagged α-subunit (indicated with an asterisk) of RNAP (lanes 5, 6, 9, and 10). Abundances were measured using Western immunoblots following protein separation via SDS−PAGE (4 to 12% acrylamide) using purified α- and β-subunits of RNAP (2.5 and 5.0 ng in lanes 1 and 2, respectively) in comparison to cellular lysates (0.5 and 1.0 μg) prepared from cells grown under aerobic (lanes 3−6) or suboxic (lanes 7−10) conditions.

are reductions in the abundances of the α- or β-subunit of RNAP. The substantially larger abundance of RNAP under aerobic growth conditions is consistent with earlier suggestions in *E. coli* where optimal growth conditions require the rapid production of stable RNA (rRNA and tRNA) necessary for ribosome assembly and protein synthesis, which are limiting under conditions associated with aerobic growth (*2*, *7*).

Expression of Tagged Proteins Induces Compensatory Degradation of the Endogenous α*-Subunit of RNAP*. To understand the cellular consequences associated with the expression of the α-subunit of RNAP, we have measured the abundances of the tagged α-subunit relative to the endogenous α- and β-subunits of RNAP. The tagged α-subunit of RNAP is apparent in Western immunoblots as a 42 kDa band above that of the endogenous 36.6 kDa protein (Figure 1). Under aerobic growth conditions, the amount of tagged α-subunit is similar to that observed for endogenous α-subunit in the empty vector control. Substantial decreases in the amount of endogenous α-subunit occur upon expression of the tagged α-subunit of RNAP, resulting in a similar overall abundance of α-subunit irrespective of the expression of the tagged protein. Under these conditions, the amount of β-subunit of RNAP is unaffected by the expression of the tagged α-subunit. These results indicate that the total protein levels of the RNAP complex are tightly regulated under aerobic conditions. In contrast, under suboxic conditions, the expression of the tagged α-subunit of RNAP has little effect on the abundance of the endogenous α-subunit, where there is a 2−3-fold increase in the total abundance of the α-subunit of RNAP relative to empty vector controls and corresponding increases in the abundance of the β-subunit of RNAP. Thus, cellular mechanisms of regulation are substantially different under aerobic or suboxic growth conditions, which maintain a constant amount of RNAP through the selective degradation of the endogenous α-subunit or increase the abundance of the β-subunit to increase the amount of RNAP, respectively. However, in both cases, the total abundance of the tagged α-subunit is near native levels and present within intact RNAP complexes, permitting the effective affinity isolation of the intact RNAP complex through the tagged α-subunit in identifying possible changes in protein binding interactions under different growth conditions.

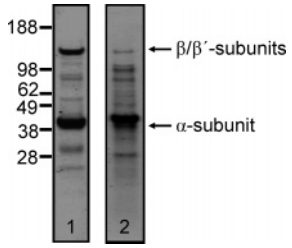

FIGURE 2: SDS−PAGE (4 to 12% acrylamide) of the isolated RNAP complex (4 μg) following the affinity isolation of the RNAP complex using either Ni-NTA beads (lane 1) or biarsenical multiuse affinity probes (MAPs) immobilized on glass beads (lane 2), as described in Experimental Procedures. LC−MS was used to identify 18 abundant proteins following affinity purification of the RNAP complex using MAPS (lane 2), which correspond to antioxidant AhpC/Tsa (SO2756, mass of 22 kDa), acetylglutamate kinase (SO0276, mass of 27 kDa), the α-subunit of RNAP (SO0256, mass of 36 or 42 kDa depending on the engineered tag), elongation factor Tu (SO0217, mass of 43 kDa), 3-oxoacyl(acyl carrier protein) synthase I (SO3072, mass of 43 kDa), serine protease HtrA/DegQ/DegS (SO3942, mass of 47 kDa), trigger factor (SO1793, mass of 48 kDa), asparaginyl-tRNA synthetase (SO2218, mass of 52 kDa), N-utilization substance protein A (SO1203, mass of 55 kDa), lysyl-tRNA synthase (SO0992, mass of 57 kDa), aspartyl-tRNA synthase (SO2433, mass of 66 kDa), chaperone protein DnaK (SO1126, mass of 69 kDa), heat shock protein HtpG (SO2016, mass of 72 kDa), homocysteine methylase (SO0818, mass of 85 kDa), clpB (SO3577, mass of 95 kDa), 2-oxoglutarate dehydrogenase (SO1930, mass of 105 kDa), the β-subunit of RNAP (SO0224, mass of 150 kDa), and the β'-subunit of RNAP (SO0225, mass of 155 kDa).

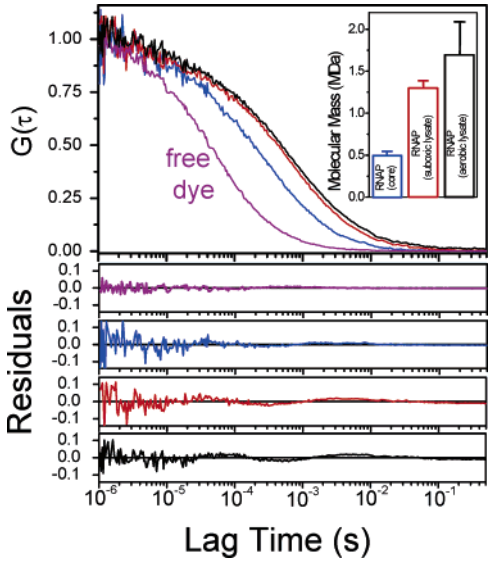

FIGURE 3: Normalized fluorescence correlation spectra of the free probe (Alexa-488; purple curve) in comparison to the labeled RNAP core enzyme (isolated using Ni-NTA) (blue curve) or the supramolecular RNAP complex in lysate obtained from *Shewanella* grown under suboxic (red curve) or aerobic (black curve) conditions. Residuals depicting differences between data and nonlinear least-squares fits are shown below respective data sets. Experimental conditions included 5 nM Alexa-488 (alone or bound to protein) in 20 mM NaH_2PO_4 (pH 7.5) or in cell lysate (8.0 mg/mL). The temperature was 20 °C.

Affinity Isolation of the RNAP Core Complex. The RNAP complex was isolated using Ni^{2+}-NTA affinity columns, which effectively bind the His_6 tag on the α-subunit, essentially as previously described (*22*). Following extensive washing with high salt (i.e., 0.5 M NaCl), the complex was eluted, and the subunit composition was analyzed by SDS−PAGE and LC−MS/MS (Figure 2). The most abundant proteins in the complex are the α-subunits that migrate as a broad band with an apparent mass of 41 ± 3 kDa, consistent with the presence of both tagged (41.7 kDa) and endogenous (36.2 kDa) α-subunits in the $\alpha_2\beta\beta'$ RNAP core complex. The β- and β'-subunits are also present, with an apparent mass of ~120 kDa, although at stoichiometries lower than that of the α-subunit. Six additional minor bands are present at stoichiometries much lower than that of the α-subunit, consistent with the presence of additional binding partners previously identified using Ni^{2+}-NTA affinity columns to isolate the RNAP complex from *E. coli* (*22*). However, in this preparation, the α-subunit of RNAP, which serves as the bait in the affinity pulldown, is the dominant protein in the isolated complex and prevents the robust identification of low-affinity binding partners that associate with RNAP in the cell.

In comparison, the isolated complex obtained using MAPs involves a one-step affinity isolation and the release of the complex using mild reducing conditions (i.e., 50 mM dithiol). The composition of the eluted RNAP protein complex is substantially larger than that obtained using the Ni^{2+}-NTA affinity isolation procedure, and 13 major bands are apparent using Coomassie blue staining following SDS−PAGE separation (Figure 2). A major band, which migrates with an apparent molecular mass of ~46 kDa just above the α-subunit, corresponds to EF-Tu, which binds nonspecifically to the bisarsenical affinity matrix (*11*). Other isolated proteins are present at stoichiometries similar to that of the α-subunit, consistent with the preservation of low-affinity binding proteins in the RNAP complex using these mild elution conditions. In comparison, we obtain few interacting proteins upon isolation of RNAP subunits from *S. oneidensis* expressed in *E. coli*, indicating that the isolated proteins in the RNAP complex isolated form *Shewanella* lysates are specific binding interactions.

Relationship between Protein Size and Translational Diffusion Coefficient. Fluorescence correlation spectroscopy (FCS) permits the determination of the size of the RNAP protein complex through the direct measurement of the translational diffusion coefficient (D_t). Using FCS, we have measured the autocorrelation curves for the free dye Alexa-488 and followed its covalent binding to the RNAP core complex isolated using Ni-NTA affinity isolation (Figure 3). Optimal nonlinear least-squares fits to the correlation curve for the free dye involved a model with one triplet state and one diffusion component, which resulted in excellent fits as evidenced by the essentially random residuals. In the case of the free dye, the triplet lifetime (τ_T) and diffusion times (τ_D) were 7.7 ± 0.8 and 64 ± 2 μs, respectively, with amplitudes of 16 and 84%, respectively. From the mass of Alexa-488, we can calculate that $D_t = 3.3 \times 10^{-10}$ m^2 s^{-1}, which is in excellent agreement with the measured value (i.e., $D_t = 3.2 \times 10^{-10}$ m^2 s^{-1}). In comparison to that of the free probe, the correlation curve for the Alexa-labeled RNAP complex obtained using an Ni^{2+}-NTA affinity purification (i.e., the core complex) is shifted toward longer times with a diffusion time of 420 ± 20 μs and a calculated molecular mass of 500 ± 50 kDa, which is consistent with the size of the core complex of $\alpha_2\beta\beta'$ (i.e., 384 kDa) and the presence of a small number of additional binding proteins (see Figure 2).

Molecular Size of the RNAP Complex in Cell Lysates. Measurements of the RNAP complex size prior to affinity isolation provide an estimate of the intact complex and were accomplished using FCS to measure the translational diffusion coefficient of fluorescently labeled RNAP following its incubation with cellular lysates obtained from *Shewanella* grown under aerobic or suboxic conditions. In comparison to the isolated core complex of RNAP obtained following affinity isolation using Ni^{2+}-NTA ($\tau_D = 420 \pm 20$ μs), there is a large shift in the correlation curve toward longer times following addition of RNAP to cellular lysates prepared from cells grown under either suboxic ($\tau_D = 770 \pm 20$ μs) or aerobic ($\tau_D = 840 \pm 70$ μs) conditions (Figure 3). Reproducibly, the correlation curves are shifted toward longer times (larger masses) for RNAP in cellular lysates from *Shewanella* grown under aerobic conditions in comparison to measurements made for RNAP in lysates from *Shewanella* grown under suboxic conditions, consistent with a larger mass of the RNAP complex. Formation of the supramolecular complex involving RNAP occurs rapidly, as the correlation times measured in the first minutes following addition of RNAP to cellular lystates are essentially identical to those observed at longer times exceeding several hours.

FCS Measurements of CaM in Shewanella Lysates for Viscosity Correction. An estimation of the apparent mass of the endogenous complex prior to affinity isolation requires a correction for the viscous nature of the cellular lysate, which was measured from a consideration of changes in the correlation curve for a eukaryotic protein (i.e., CaM) added to cellular lysates, which is not expected to bind to bacterial proteins. CaM is a eukaryotic calcium signaling protein, which we used as a control to assess nonspecific effects related to the increased viscosity of *Shewanella* lysate and nonspecific protein associations. In comparison to that of the free probe, the correlation curve for Alexa-labeled CaM is shifted toward longer times with diffusion time of 230 $\pm$ 10 μs, which is consistent with the larger mass (Figure 4). The calculated diffusion coefficient (D_t) from the FCS measurement is 1.0×10^{-10} m^2 s^{-1} for CaM, which is in close agreement with the theoretical value of 0.9×10^{-10} m^2 s^{-1} for calcium-activated CaM calculated from the crystal structure of PDB entry 1cll using Hydropro (*23*), providing confidence that the measured translational diffusion coefficients provide an accurate measurement of the macromolecule size. Inspection of the correlation curves for isolated CaM relative to that in cellular lysates shows they are very similar; nevertheless, the diffusion time increases by 32% from 230 $\pm$ 10 μs for isolated CaM to 304 $\pm$ 11 μs for CaM added to *Shewanella* lysate.

Upon correction for this viscosity effect, the apparent mass of the RNAP complex in lysate was between 1.4 $\pm$ 0.1 and 1.7 $\pm$ 0.4 MDa, depending on growth conditions. The large mass of the RNAP complex in cellular lysates is substantially greater than would be expected from binding interactions involving the core complex with σ factors and suggests that additional proteins bind RNAP.

LC−MS/MS Identification of the RNAP Complex. Using LC−MS, we have identified the proteins that elute with the RNAP complex following affinity isolation of the α-subunit of RNAP using newly developed MAPs in comparison to control samples containing an empty vector control. Using lysates from *Shewanella* grown under aerobic and suboxic conditions, affinity pulldowns were repeated three times under each growth condition. Each sample was measured in triplicate for a total of 36 LC−MS/MS measurements. Peptide identifications used previously validated SEQUEST filters, fully described in the Supporting Information. To rapidly identify proteins that are copurified with the α-subunit of RNAP that may be present at near-stoichiometric amounts, we used a visual clustering approach to correlate abundance changes of isolated proteins (i.e., $\langle X_{corr} \rangle$) associated with affinity purification of the complex (Figure 5). Subsequent analysis of quantitative protein abundance changes relative to control (i.e., no bait) samples was used to identify additional binding interactions with the RNAP complex that may be present at lower molar stoichiometries (Figure 6).

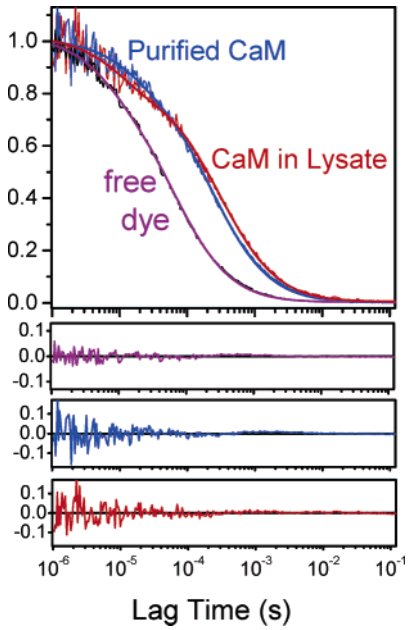

FIGURE 4: Normalized fluorescence correlation spectra (thin lines) and nonlinear least-squares fits (thick lines) for the free probe (Alexa-488; purple curve) in comparison to Alexa-labeled CaM alone (blue curve) or following addition into *Shewanalla* lysate (8.0 mg/mL). Residuals depicting differences between data and nonlinear least-squares fits are shown for each data set. Experimental conditions included 5 nM Alexa-488 (alone or bound to protein) in 20 mM NaH_2PO_4 (pH 7.5) or upon addition to *Shewanella* lysate at 20 °C.

Visual Clustering of Isolated Proteins that Are Copurified with RNAP. The RNAP core subunits (i.e., α, β, and β') were found under all growth conditions, as was the initiation factor IF-2α that mediates the formylation-independent transcription and subsequent activation of RNAP associated with the transcription of stable RNA (*24*). In addition, 21 proteins were identified as part of the central RNAP complex under aerobic growth conditions; in comparison, only four proteins in addition to the core complex were identified in association with the RNAP complex under suboxic growth conditions. The substantial changes in the complex identified under aerobic and suboxic growth conditions suggest that changes in the RNAP complex may contribute to the cellular response to environmental conditions involving the reprogramming of RNAP to switch from the primary synthesis of stable RNA (i.e., tRNA and mRNA) to the enhanced synthesis of mRNA as part of a global reprogramming to increase the metabolic diversity of the organism (*25*). Of the 25 proteins identified

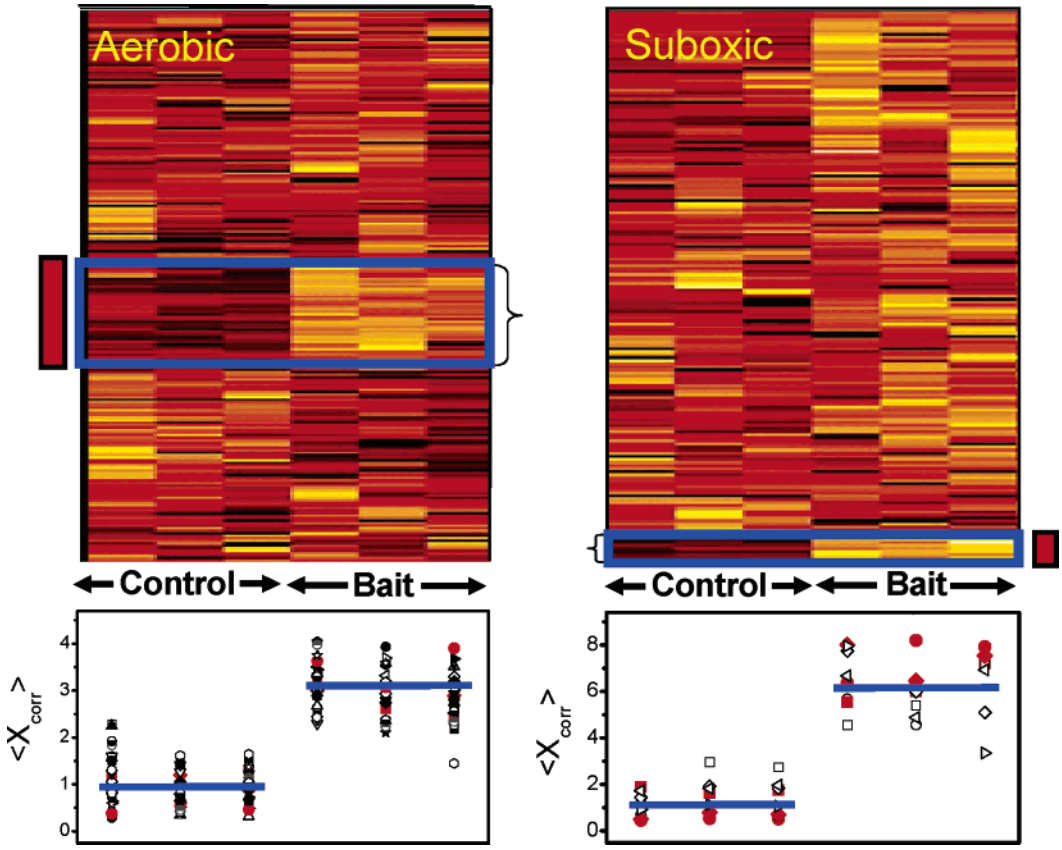

FIGURE 5: Identification of proteins that are copurified with RNAP isolated from lysates expressing the α-subunit of RNAP relative to empty vector controls grown under aerobic (left) or suboxic (right) conditions, based on correlated abundance changes in identified proteins visualized as a heat map using OmniViz to cluster the data (proteins that are copurified with RNAP are highlighted in the blue box). Columns represent individual LC−MS measurements of isolated complexes, while rows represent the relative abundances of identified proteins (i.e., $\langle X_{corr} \rangle$; see eq 1 in Experimental Procedures). Bottom panels depict correlated abundance changes of proteins that are copurified with RNAP. Under aerobic conditions, besides the core complex, 22 additional binding partners are observed, while under suboxic conditions, only five additional proteins were found in addition to the core complex. Proteins and associated $\langle X_{corr} \rangle$ values for proteins in the RNAP complex identified include the RNAP core enzymes (found under all conditions), DNA-directed RNA polymerase α-subunits (red) [SO0256 (●)], the DNA-directed RNA polymerase *β*-subunit [SO0224 (■)], and the DNA-directed RNA polymerase *β′*-subunit [SO0225 (◆)] as well was proteins that are copurified with RNAP (see the bottom panels), which under aerobic conditions (bottom left panels) include ribosomal protein L10 [SO0222 (◒)], acetylglutamate kinase [SO0276 (★)], amidase family protein [SO0888 (empty rightward-pointing triangle)], lysyl-tRNA synthetase [SO0992 (●)], chaperone protein DnaK [SO1126 (▽)], N-utilization substance protein A [SO1203 (■)], translation initiation factor IF-2 [SO1204 (○)], trigger factor [SO1793 (▼)], AMP-binding family protein [SO1971 (empty leftward-pointing triangle)], adenylate kinase [SO2018 (◓)], asparaginyl-tRNA synthatase [SO2218 (▲)], aspartyl-tRNA synthatase [SO2433 (◇)], phosphate acetyltransferase [SO2916 (△)], the oxidoreductase short-chain dehydrogenase/reductase family [SO2935 (⬟)], 3-oxoacyl(acyl carrier protein) synthase I [SO3072 (filled leftward-pointing triangle)], the electron transfer flavoprotein α-subunit [SO3144 (☆)], the electron transfer flavoprotein *β*-subunit [SO3145 (⬠)], polysaccharide biosynthesis protein [SO3189 (⬡)], flagellar motor switch protein FliG [SO3227 (filled rightward-pointing triangle)], clpB protein [SO3577 (▲)], sulfate adenylyltransferase subunit 2 [SO3727 (⬢)], and the serine protease HtrA/DegQ/DegS family [SO3942 (◆)]. Under suboxic conditions, proteins and associated $\langle X_{corr} \rangle$ values (see the bottom right panels) include the DNA gyrase B subunit [SO0011 (○)], nitrogen regulatory protein P-II 1 [SO0761 (◇)], translation initiation factor IF-2 [SO1204 (empty leftward-pointing triangle)], OmcA [SO1779 (□)], and the formate dehydrogenase α-subunit [SO4513 (empty rightward-pointing triangle)].

to bind to the RNAP core complex under either growth condition, 15 of these proteins had been previously suggested to interact with RNAP (see Table S1 of the Supporting Information).

Proteins found to associate with RNAP under aerobic conditions include DnaK, trigger factor, and clpB, which are known to associate with each other and regulate transcription of RNAP through a chaperone activity that modulates, for example, the stabilization of σ^{32} (*26*). In addition, the known RNAP regulator NusA was found, which tightly binds to RNAP under conditions of rapid growth to promote the greater transcriptional rate of stable RNA (in comparison to mRNA where pausing is common) (*27*). Environmental sensors known to mediate metabolic changes in response to growth conditions found in association with RNAP include acetylglutamate kinase and FliG (*28*, *29*). Additional bound subunits include the cytosolic portions of membrane proteins associated with energy metabolism and ATP synthesis (e.g., AMP-binding protein, phosphate acetyltransferase, and electron transfer proteins with links to dehydrogenases), consistent with recent structural data demonstrating the membrane localization of RNAP under optimal growth conditions, where the majority of RNAP is densely associated with the seven operons encoding stable RNA (*4*). These results suggest that the association between RNAP and metabolic enzymes may facilitate diffusion-limited reactions associated with transcription.

Consistent with this latter suggestion, under suboxic conditions when transcriptional rates are no longer limiting, we find that many fewer proteins associate with RNAP.

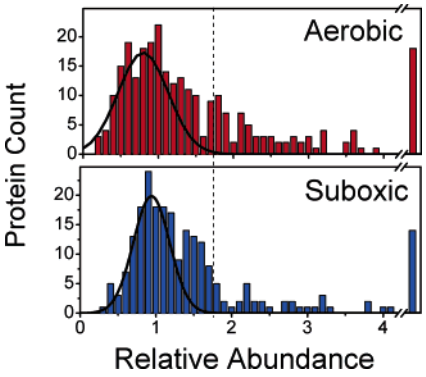

FIGURE 6: Histogram depicting relative abundances of identified proteins that are copurified with the RNAP complex from lysates prepared from *Shewanella* grown under aerobic (red) or suboxic (blue) conditions. The normal distribution (black line) corresponds to background proteins equally abundant in both bait and control experiments.

Associations are observed between RNAP and DNA gyrase, formate dehydrogenase subunit α, nitrogen regulatory protein P−II, and OmcA. DNA gyrase has previously been reported to copurify with RNAP and to enhance transcription (*30*). Formate dehydrogenase subunit α (SO4513) is part of a membrane protein complex linked to nitrite respiratory pathways under anaerobic conditions, where formate produced from lactate serves as a major donor of electrons to a variety of inducible respiratory pathways that use terminal electron acceptors other than molecular oxygen (*31*). The linkage between diverse energy sources and RNAP is consistent with the observed association between nitrogen regulatory protein P-II (links to Ntr and σ factor regulation) and OmcA (functions to couple anaerobic metabolism to the reduction of extracellular metals) (*32*).

Quantitative Analysis of Relative Protein Abundances. Additional proteins that may associate weakly with the RNAP complex to regulate function were identified through a consideration of their abundances relative to the control sample transformed with the empty vector. These protein identifications are important, as low-affinity interactions have previously been suggested to target RNAP to specific promoters and enhance transcriptional rates and are critical to our understanding of the regulation of RNAP (*8*, *9*). Confident identification of a protein required observation of each of the three biological replicates involving the affinity isolation of the complex. A total of 341 unique proteins were identified in the replicate pulldowns of the RNAP under both suboxic and aerobic conditions, whose relative abundances varied between those similar to the control sample and those that were present in relatively high abundances (Figure 6).

From a consideration of their relative abundances, it is apparent that many proteins associate nonspecifically with the affinity matrix and are not part of the RNAP complex. The population of nonspecifically bound proteins can be described by a normal probability distribution centered near unity. Only identified proteins whose relative abundances are greater than 1.7 can be unambiguously assigned to be part of the RNAP complex. Of the proteins identified to copurify with RNAP, we find that 91 are present under aerobic growth conditions and 47 are present under suboxic growth conditions. These results suggest that there are large changes in the RNAP complex as part of the cellular response to changing environmental conditions. The identified proteins

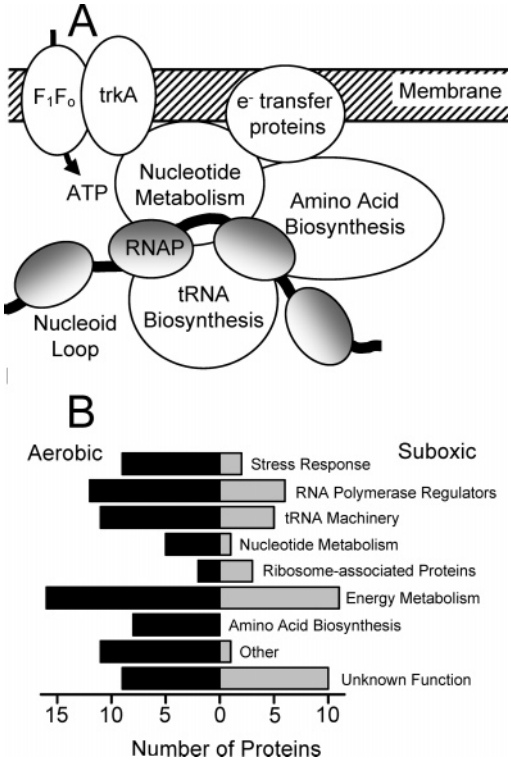

FIGURE 7: (A) Cartoon depicting the suggested organization of RNAP in complex with metabolic enzymes and (B) changes in functional categories for proteins that copurify with the RNAP complex under aerobic (black bars) or suboxic (gray bars) growth conditions (see Table 1). The indicated association between trkA and F_1F_0 is consistent with prior suggestions (*54*).

are present at substoichiometric levels, which is apparent from a comparison of the measured mass of the RNAP supramolecular complex (i.e., 1.4 and 1.7 MDa under suboxic and aerobic conditions; see Figure 3) relative to that calculated assuming equimolar stoichiometries of all isolated proteins (i.e., 2.5 and 4.3 MDa under suboxic and aerobic conditions). Because only five ribosomal proteins were identified, these results indicate that we have effectively isolated the core complex free of nonspecific binding interactions involving associated polysomes commonly observed in prior pulldowns (*33*).

DISCUSSION

We find that RNA polymerase exists as a large supramolecular complex with an apparent mass in excess of 1.4 MDa (Figure 3) that undergoes significant changes in subunit composition (remodeling) in response to environmental growth conditions (Figure 7). In comparison to suboxic conditions, a larger number of binding partners associate with RNAP under aerobic conditions (Table 1 and Figure 7), where cellular growth rates are limited by the rates of ribosome biosynthesis (*2*, *7*). In addition to known regulators of RNAP function, binding partners include a surprisingly large number of metabolic enzymes associated with ATP synthesis, nucleotide metabolism, and the biosynthesis of stable RNA (i.e., tRNA and rRNA; Figure 7). Our identification of cytosolic subunits of membrane proteins with the RNAP complex (Table 1) is consistent with recently published structural data demonstrating the membrane localization of RNAP in rapidly growing cells (*4*). In contrast, under suboxic conditions, we observe a reduced number of

Table 1: Identified Proteins that Copurify with RNAP under Aerobic or Suboxic Growth Conditions

gene	symbol	common name	identification aerobic	identification suboxic
(A) core complex				
SO0224	*rpoB*	RNA polymerase β	X	X
SO0225	*rpoC*	RNA polymerase β'	X	X
SO0256	*rpoA*	RNA polymerase α	X	X
(B) stress response proteins (14)				
SO0052	*secB*	protein export protein SecB	X	
SO0874	*dksA*	DnaK suppressor protein		X
SO1065	*fkpA*	peptidyl-prolyl cis−trans isomerase FkpA	X	
SO1126	*dnaK*	chaperone protein DnaK (Hsp70)	X	
SO1139	*fklB*	peptidyl-prolyl cis−trans isomerase FklB	X	
SO1793	*tig*	trigger factor	X	
SO2267	*hscB*	cochaperone Hsc20	X	X
SO3417	*slyD*	peptidyl-prolyl cis−trans isomerase SlyD	X	X
SO3577	*clpB*	clpB protein	X	X
SO3637	*surA*	survival protein surA	X	
SO4211	*secA*	preprotein translocase SecA subunit	X	
SO4405	*katG-2*	catalase/peroxidase HPI		X
SO4507		TorA specific chaperone putative	X	
SO4640		antioxidant AhpC/Tsa family	X	
(C) RNA polymerase regulators (19)				
SO0011	*gyrB*	DNA gyrase B subunit		X
SO0219	*nusG*	transcription antitermination protein NusG	X	
SO0276	*argB*	acetylglutamate kinase	X	
SO0761	*glnB-1*	nitrogen regulatory protein P-II 1		X
SO0769	*argR*	arginine repressor		X
SO1203	*nusA*	N-utilization substance protein A	X	
SO1204	*infB*	translation initiation factor IF-2	X	X
SO1938	*cobB*	cobB protein	X	
SO1946	*phoP*	transcriptional regulatory protein PhoP	X	
SO2347	*gapA-3*	glyceraldehyde-3-PO_4 dehydrogenase	X	
SO3202	*cheW-3*	purine-binding chemotaxis protein CheW		X
SO3210	*fliA*	RNA polymerase σ-27 factor		X
SO3227	*fliG*	flagellar motor switch protein FliG	X	
SO3519	*glnB-2*	nitrogen regulatory protein P-II 1	X	
SO3982		DNA-binding response regulator	X	
SO3988	*arcA*	aerobic respiration control protein ArcA	X	
SO4428		DNA-binding response regulator		X
SO4633	*ompR*	transcriptional regulatory protein OmpR	X	
SO4647		DNA-binding response regulator	X	
(D) tRNA machinery (17)				
SO0196	*selD*	selenophosphate synthetase		X
SO0217	*tufB*	translation elongation factor Tu	X	
SO0294	*trpS*	tryptophanyl-tRNA synthetase		X
SO0818	*metE*	homocysteine methylase, pterin-dep	X	
SO0992	*lysS*	lysyl-tRNA synthetase	X	X
SO1181	*miaB*	tRNA-i(6)A37 modification enzyme MiaB	X	
SO1261		mercaptopyruvate sulfurtransferase	X	
SO1676	*metA*	homoserine *O*-succinyltransferase	X	
SO2218	*asnS*	asparaginyl-tRNA synthetase	X	
SO2264	*iscS*	cysteine desulfurase		X
SO2433	*aspS*	aspartyl-tRNA synthetase	X	
SO3070	*asd*	aspartate semialdehyde dehydrogenese		X
SO3312	*ispG*	HDMAPP synthase	X	
SO3428	*alaS*	alanyl-tRNA synthetase		X
SO3532	*ileS*	isoleucyl-tRNA synthetase	X	
SO3727	*cysD*	sulfate adenylyltransferase subunit 2	X	
SO3736	*cysH*	PAPS reductase	X	
(E) nucleotide metabolism (7)				
SO1150	*rpiA*	ribose-5-phosphate isomerase	X	
SO1268		glutamine synthetase	X	
SO2018	*adk*	adenylate kinase	X	
SO2760	*purM*	FGAM cyclo-ligase	X	
SO2834	*nrdD*	anaerobic rNTP reductase		X
SO3293	*guaB*	IMP dehydrogenase	X	X
SO4410	*glnA*	glutamine synthetase type I	X	
(F) ribosome-associated proteins (5)				
SO0220	*rplK*	ribosomal protein L11	X	
SO0222	*rplJ*	ribosomal protein L10	X	
SO1632	*frr*	ribosome recycling factor		X
SO2328	*efp*	translation elongation factor P		X
SO4094	*cafA*	ribonuclease G		X
(G) energy metabolism (29)				
SO0029	*trkA*	potassium uptake protein TrkA	X	
SO0398	*frdA*	fumarate reductase flavoprotein		X
SO0770	*mdh*	malate dehydrogenase		X
SO0840		acetyl-CoA carboxylase accADC α	X	
SO0968	*ldhA*	D-lactate dehydrogenase		X
SO1016	*nuoG*	NADH dehydrogenase I G subunit	X	
SO1017	*nuoF*	NADH dehydrogenase I F subunit		X
SO1019	*nuoCD*	NADH dehydrogenase I C/D subunits		X
SO1484	*aceA*	isocitrate lyase		X
SO1640	*fabZ*	(3*R*)-hydroxymyristoyl-ACP dehydratase	X	
SO1779	*omcA*	decaheme cytochrome *c*		X
SO1928	*sdhA*	succinate dehydrogenase flavoprotein	X	
SO1929	*sdhB*	succinate dehydrogenase iron−sulfur protein		X
SO1932	*sucC*	succinyl-CoA synthase β-subunit	X	
SO1971		AMP-binding family protein	X	
SO2222		fumarate hydratase class I, anaerobic, putative	X	
SO2339		α-ketoacid dehydrogenase complex E1	X	X
SO2483		aspartate aminotransferase putative	X	
SO2743	*acs*	acetyl-coenzyme A synthetase	X	
SO2778	*fabH-1*	3-oxoacyl(acyl carrier protein) synthase III	X	
SO2916	*pta*	phosphate acetyltransferase	X	X
SO2935		oxidoreductase, short-chain	X	
SO3072	*fabB*	3-oxoacyl(acyl carrier protein) synthase I	X	
SO3144	*etfA*	electron transfer flavoprotein α	X	
SO3145	*etfB*	electron transfer flavoprotein β	X	
SO3664	*fadD-2*	long-chain fatty acid-CoA ligase	X	
SO3991	*fbp*	fructose 16-bisphosphatase		X
SO4513		formate dehydrogenase α-subunit		X
SOA0060		acetyltransferase GNAT family		X
(H) proteins of unknown function (19)				
SO0554		hypothetical protein	X	
SO0568		conserved hypothetical protein		X
SO0783		hypothetical protein	X	
SO0795		conserved hypothetical protein		X
SO1227		conserved hypothetical protein	X	
SO1581	*phnA*	phnA protein	X	
SO1722		ACT domain protein		X
SO2177		conserved hypothetical protein	X	
SO2241		conserved hypothetical protein		X
SO2407		conserved hypothetical protein	X	
SO2586		conserved hypothetical protein		X
SO2929		hypothetical protein	X	
SO3775		hypothetical protein		X
SO3856		hypothetical protein		X
SO3915		conserved hypothetical protein		X
SO4476	*spy*	spheroplast protein y precursor, putative	X	
SOA0059		conserved hypothetical protein		X
SOA0080		hypothetical protein		X
SOA0110		lipoprotein, putative	X	
(I) amino acid biosynthesis (9)				
SO0287	*aroB*	3-dehydroquinate synthase	X	
SO0888		amidase family protein	X	
SO1367	*pheA*	chorismate mutase/prephenate dehydratase	X	
SO3079	*aroC*	chorismate synthase, authentic frameshift	X	
SO3413	*thrC*	threonine synthase	X	
SO3760	*glnE*	glutamine-synthetase adenylyltransferase		X
SO3986	*lysC*	aspartokinase III, lysine-sensitive	X	
SO4309	*lysA*	diaminopimelate decarboxylase	X	
SO4480	*aldA*	aldehyde dehydrogenase	X	
(J) other functions (11)				
SO1209	*pnp*	polyribonucleotide nucleotidyltransferase	X	
SO1252		peptidase U32 family	X	
SO1680		enoyl-CoA hydratase/isomerase	X	
SO1870	*speA*	biosynthetic arginine decarboxylase	X	
SO2445	*thiC*	thiamin biosynthesis protein ThiC	X	
SO2907		TonB-dependent receptor domain protein	X	
SO3189		polysaccharide biosynthesis protein	X	
SO3545		OmpA family protein	X	
SO3942		serine protease HtrA/DegQ/DegS family	X	
SO4687	*ugd*	UDP-glucose 6-dehydrogenase	X	
SO4699	*prlC*	oligopeptidase A	X	

protein associations, which is consistent with the observed disruption of RNAP in condensed structures near the membrane under suboptimal growth conditions (*4*). Indeed, under conditions that limit growth, there is a substantial redistribution of RNAP to promoters associated with the transcription of mRNA whose initiation and elongation rates are much slower than those associated with the transcription of stable RNA. These results suggest that the structural

coupling between RNAP and identified metabolic enzymes functions as an organizing center at the membrane, which acts to increase the local concentrations of all necessary substrates to enhance the efficiency of RNAP. In comparison, under suboptimal conditions, there is a redistribution of RNAP to promoters associated with mRNA, where transcriptional rates do not limit cell growth.

Relationship between Prior Work and Identified Proteins that Are Copurified with RNAP. Of the 130 identified RNAP-binding proteins, 91 have associated gene symbols and could thus be readily compared with previously identified RNAP binding interactions; 59 of these proteins (i.e., 65%) have previously been identified to associate with bacterial RNAP either experimentally (28 proteins) or using publicly available experimental and predictive databases (47 proteins) (see Table S1 of the Supporting Information). Of the previously identified binding partners, 11 (38%) have previously been purified and rigorously validated, including (i) stress response proteins DnaK suppressor protein and chaperone protein DnaK, (ii) RNAP regulators DNA gyrase, transcription antitermination protein NusG, arginine repressor, N-utilization substance protein A (NusA), transcription initiation factor IF-2, α factor 27 (FliA), and transcriptional regulatory protein OmpR (*34*), and (iii) tRNA machinery translation elongation factor Tu. In addition, while not previously reported in prokaryotes, eukaryotic glyceraldehyde-3-phosphate dehydrogenase is known to associate with RNAP (see Table S1 of the Supporting Information). Two proteins (i.e., the Sir2 family protein cobB and the transcriptional regulator PhoP) were previously known to regulate RNAP and to associate with DNA, but prior to our measurements, their interaction with RNAP had not been identified. Likewise, genetic screens have identified functional linkages between numerous tRNA synthetases and RNAP function (*35*, *36*). However, no prior measurements were able to document the extensive range of binding partners that simultaneously associate with RNAP.

Comparison of Methods for Identification of Protein Complexes. Multiple complementary approaches were used in the identification of proteins associated with the RNAP supramolecular complex, which involved (i) protein complex isolation and the identification of isolated proteins using SDS−PAGE and LC−MS (Figure 2), (ii) the use of visual clustering algorithms in rapidly identifying proteins that copurify with RNAP (Figure 5), and (iii) a quantitative measure of abundances relative to control samples transformed with an empty vector that permits the identification of low-affinity binding partners (Figure 6). Using SDS−PAGE in combination with the biarsenical affinity column, 13 distinct bands are apparent following the purification of the RNAP complex, which were identified by LC−MS/MS to contain 18 proteins (see the legend of Figure 2). Of the 18 identified proteins, we found that 15 were consistently present above background as part of the RNAP complex, as indicated in Table 1.

None of the proteins that nonspecifically associate with the RNAP complex identified in the analysis of the SDS−PAGE data (i.e., SO2756, SO2016, and SO1930) were observed using the OmniViz clustering algorithm (Figure 5). Of the 15 proteins identified on the SDS−PAGE gels that were determined to be part of the RNAP complex, 13 were also identified using the OmniViz clustering algorithm (which identified a total of 22 proteins that copurify with the RNAP core complex under aerobic conditions). Only elongation factor Tu (SO0217) and homocysteine methylase (SO0818) were not found using the OmniViz clustering algorithm. In the case of elongation factor Tu, this is understandable as large amounts of this protein bound nonspecifically to the resin, obscuring the proportional increase in abundance associated with the purification of RNAP used in the OmniViz algorithm. Overall, these results indicate that the OmniViz clustering approach provides a rapid means of identifying copurifying proteins that may be present at near stoichiometric amounts in the RNAP supramolecular complex. In comparison, a total of 91 proteins are found to copurify with the RNAP supramolecular complex using a quantitative analysis in which modest differences in enrichment are detected to identify proteins (Figure 6). This latter analysis of proteins likely to associate with RNAP is based on a probabilistic distribution of binding interactions, and in the absence of additional validation schemes, there is some uncertainty for any single protein regarding the binding with the RNA polymerase complex. Nevertheless, these results indicate that RNAP exists as a large supramolecular complex and provide a high-level understanding of the role of low-affinity binding interactions that can function to increase the abundance of metabolites associated with RNAP function (Figure 7). Through a comparison of these different complementary analysis methods, we suggest a means of identifying high-affinity protein associations in the RNAP supramolecular complex that are present at near stoichiometric abundances from low-affinity binding interactions whose relative abundances are reduced.

Increased Abundance of the Stress Response Protein in Complex with RNAP under Aerobic Conditions. Under aerobic growth conditions (where significant oxidative stress occurs), 12 stress response proteins (largely chaperones) are present in complex with RNAP (Table 1 and Figure 7), including the major bacterial chaperone system involving the Hsp70 bacterial analogue DnaK (SO1126) and its chaperone binding partners clpB (SO3577) and trigger factor (SO1793), which are known to mediate heat shock transcriptional responses (*26*). In addition, other chaperones include sec B (SO0052) and two peptidyl-prolyl cis−trans isomerases known to be members of a multiprotein complex (*37*, *38*), cochaperone Hsc20 (SO2267), SlyD, and SurA. In comparison, under suboxic conditions, DnaK suppressor protein (SO0874) and three chaperones are present in association with RNAP, consistent with the global reprogramming of transcriptional activity in downregulating the abundance of chaperones and heat shock proteins.

Regulators of RNAP Function. Different regulators of RNAP activity associate with the RNAP complex in response to aerobic or suboxic conditions. Under aerobic conditions, RNAP binders include NusA (SO1203), which is known to compete with σ^{70} and to modulate transcriptional pausing (*39*), antitermination factor NusG (SO0219), transcription regulator cobB (SO1938), glyceraldehyde-3-phosphate dehydrogenase (GAPDH) (SO2347), which is known to activate eukaryotic RNAP (*40*), and IF-2 (SO1204), which promotes the transcription of stable RNA (*24*). Multiple proteins that function as part of two-component regulatory sensors are observed, including OmpR (SO4633), ArcA (SO3988), PhoP (SO1946), FliG (SO3227), and DNA-

binding response regulators SO3982 and SO4647 (see Table 1). In addition, the nitrogen regulatory sensor protein PII-1 (SO3519) and its binding partner SO0276 are present, indicating a linkage between nitrogen regulatory sensing and transcription (*41*, *42*). In comparison, under suboxic conditions, regulators associated with RNAP include those linked to cellular motility and chemotaxis (*43*) and include σ factor FliA (SO3210) and CheW (SO3202). These results are consistent with prior observations that under optimal growth conditions a majority of RNAP associates with operons involving the transcription of stable RNA, the biosynthesis of which limits bacterial growth (*25*).

Functional Association between tRNA Machinery and RNAP. Consistent with the expectation that a multiprotein complex associating with RNAP will contain necessary proteins associated with ribosomal biosynthesis, six aminoacyl tRNA synthetases are observed in complex with RNAP. In addition, a large number of proteins associated with tRNA base modification are observed, including MiaB (SO1181) and its binding partner ispG (SO3312) that are associated with isopentenylated A37 base modification of tRNA near the anticodon region that is necessary for initiation (*44*−*46*), PAPS reductase (SO3736), cysD (SO3727), mercaptopyruvate sulfurtransferase (SO1261), selenophosphate synthetase (SO0196), cysteine desulfurase (SO2264), and aspartate semialdehyde dehydrogenase (SO3070). These binding partners would have the effect of increasing local concentrations of mature tRNA to increase rates of protein biosynthesis. Indeed, abundances of tRNA (and rRNA) can limit rates of *E. coli* growth, requiring cells to adjust growth rates to generate sufficient ribosomes. Other binding partners include EF-Tu (SO0217), which associates with tRNA and promotes RNAP polymerase activity (*47*), the transcriptional activator met E (SO0818), whose binding to DNA is necessary for the activation of some genes (*48*), and the protein metA (SO1676) associated with heat shock transcriptional regulation (*41*). Together, these protein components will have the effect of increasing rates of stable RNA and ribosomal protein biosynthesis to facilitate optimal cell growth.

Nucleotide Metabolism and RNAP. Prior results demonstrate that the rate of transcription initiation by RNAP is directly proportional to the concentration of ATP (regulated by metabolic activity) (*49*). Indeed, stable RNA promoters have a particularly high K_m for initiation through RNAP and are highly sensitive to a declines in purine abundances, which are selectively downregulated under poor growth conditions (*25*). Thus, the copurification of seven proteins associated with nucleotide metabolism with RNAP has the potential to enhance transcriptional rates through the maintenance of nucleotide concentrations. Indeed, a majority of the isolated proteins linked to nucleotide metabolism (i.e., 85%) associate with RNAP under aerobic conditions, and 70% are directly associated with purine (e.g., adenosine) biosynthesis and have the potential to directly regulate RNAP activity in addition to providing the needed substrates for polymerase activity. In addition, a large number (i.e., 11) of additional proteins (i.e., Table 1; other functions) are observed to associate with RNAP under aerobic growth conditions, which are dominated by endonucleases and proteases, many of which are required for cell growth and are associated with transcriptional regulation (*50*−*52*).

Physiological Significance. Broadly, our results are consistent with prior suggestions that considerable rate enhancements in transcriptional activity can be caused by the regulated recruitment of multiple proteins to enhance association of RNAP with relevant promoters (*8*, *9*). However, in addition to the active unit directly associated with polymerase activity, our results indicate an increased abundance of metabolic enzymes associated with ATP generation, tRNA processing, and nucleotide metabolism under aerobic conditions, where the transcription of stable RNA and ribosomal proteins are rate-limiting steps with respect to cell growth (*25*). Indeed, any shortage in the abundance of charged amino-acyl tRNA has important consequences in limiting transcription (i.e., the rate of rRNA synthesis is proportional to the rate of protein synthesis), and a shortage of any species of amino acid-charged tRNA (usually a result of poor growth conditions) that limits the rate of protein synthesis triggers a sweeping metabolic readjustment through the action of RelA synthetase activity as part of the stringent response (*25*, *53*). Consistent with this requirement, we observe that nine enzymes associated with amino acid biosynthesis are copurified with RNAP under aerobic growth conditions (Table 1). Indeed, a major facet of RNAP regulation in the absence of sufficient amounts of amino acid-charged tRNA is an abrupt 90−95% reduction in the rate of rRNA and tRNA synthesis and the depression of other metabolic processes (DNA replication, nucleotide biosynthesis, and energy metabolism) that is concurrent with upregulation of others (such as amino acid biosynthesis). In rapidly growing cells, RNAP molecules are densely packed inside the rRNA and tRNA operons, where ~80% of the active RNAP molecules synthesize stable RNA (tRNA and rRNA), which are encoded by genes that represent less than 1% of the genome (*2*). Under these conditions, no additional rate enhancements are possible through the recruitment of more RNAP to bind to relevant promoters. However, ribosome biosynthesis is tightly regulated, and there are rapid adjustments with respect to the fraction of RNAP associated with stable RNA biosynthesis and corresponding increases in the diversity of gene expression under diminished growth conditions (*7*). Our results identify a structural coupling between RNAP and metabolic enzymes associated with the generation of all necessary substrates for RNAP function, which will function to enhance RNAP function under highly favorable conditions where initiation and elongation rates of polymerase activity have already approached their maximal values.

ACKNOWLEDGMENT

We thank Joshua N. Adkins, James K. Fredrickson, Samuel O. Purvine, and Liang Shi for insightful discussions. Technical assistance was provided by Eric A. Hill in the controlled cultivation of *Shewanella*, Julie M. Gephardt in technical editing, and the EMSL proteomics facility in mass spectrometric analysis.

SUPPORTING INFORMATION AVAILABLE

Conditions associated with the cultivation of both empty vector controls and *Shewanella* expressing a tagged α-subunit of RNAP (Figure S1) and proteins identified via copurification of RNAP from lysates of *Shewanella* grown under

aerobic or suboxic conditions (Table S1). This material is available free of charge via the Internet at http://pubs.acs.org.

REFERENCES

1. Nealson, K. H., and Saffarini, D. (1994) Iron and manganese in anaerobic respiration: Environmental significance, physiology, and regulation, *Annu. Rev. Microbiol. 48*, 311−343.
2. Cabrera, J. E., and Jin, D. J. (2003) The distribution of RNA polymerase in *Escherichia coli* is dynamic and sensitive to environmental cues, *Mol. Microbiol. 50*, 1493−1505.
3. Cabrera, J. E., and Jin, D. J. (2006) Active transcription of rRNA operons is a driving force for the distribution of RNA polymerase in bacteria: Effect of extrachromosomal copies of rrnB on the in vivo localization of RNA polymerase, *J. Bacteriol. 188*, 4007−4014.
4. Jin, D. J., and Cabrera, J. E. (2006) Coupling the distribution of RNA polymerase to global gene regulation and the dynamic structure of the bacterial nucleoid in *Escherichia coli*, *J. Struct. Biol. 156*, 284−291.
5. Beliaev, A. S., Klingeman, D. M., Klappenbach, J. A., Wu, L., Romine, M. F., Tiedje, J. M., Nealson, K. H., Fredrickson, J. K., and Zhou, J. (2005) Global transcriptome analysis of *Shewanella oneidensis* MR-1 exposed to different terminal electron acceptors, *J. Bacteriol. 187*, 7138−7145.
6. Kolker, E., Picone, A. F., Galperin, M. Y., Romine, M. F., Higdon, R., Makarova, K. S., Kolker, N., Anderson, G. A., Qiu, X., Auberry, K. J., Babnigg, G., Beliaev, A. S., Edlefsen, P., Elias, D. A., Gorby, Y. A., Holzman, T., Klappenbach, J. A., Konstantinidis, K. T., Land, M. L., Lipton, M. S., McCue, L. A., Monroe, M., Pasa-Tolic, L., Pinchuk, G., Purvine, S., Serres, M. H., Tsapin, S., Zakrajsek, B. A., Zhu, W., Zhou, J., Larimer, F. W., Lawrence, C. E., Riley, M., Collart, F. R., Yates, J. R., III, Smith, R. D., Giometti, C. S., Nealson, K. H., Fredrickson, J. K., and Tiedje, J. M. (2005) Global profiling of *Shewanella oneidensis* MR-1: Expression of hypothetical genes and improved functional annotations, *Proc. Natl. Acad. Sci. U.S.A. 102*, 2099−2104.
7. Liu, M., Durfee, T., Cabrera, J. E., Zhao, K., Jin, D. J., and Blattner, F. R. (2005) Global transcriptional programs reveal a carbon source foraging strategy by *Escherichia coli*, *J. Biol. Chem. 280*, 15921−15927.
8. Ptashne, M. (2003) Regulated recruitment and cooperativity in the design of biological regulatory systems, *Philos. Trans. R. Soc. London, Ser. A 361*, 1223−1234.
9. Ptashne, M., and Gann, A. (1997) Transcriptional activation by recruitment, *Nature 386*, 569−577.
10. Ozaki, M., Wada, A., Fujita, N., and Ishihama, A. (1991) Growth phase-dependent modification of RNA polymerase in *Escherichia coli*, *Mol. Gen. Genet. 230*, 17−23.
11. Mayer, M. U., Shi, L., and Squier, T. C. (2005) One-step, nondenaturing isolation of an RNA polymerase enzyme complex using an improved multi-use affinity probe resin, *Mol. BioSyst. 1*, 53−56.
12. Fang, R., Elias, D. A., Monroe, M. E., Shen, Y., McIntosh, M., Wang, P., Goddard, C. D., Callister, S. J., Moore, R. J., Gorby, Y. A., Adkins, J. N., Fredrickson, J. K., Lipton, M. S., and Smith, R. D. (2006) Differential label-free quantitative proteomic analysis of *Shewanella oneidensis* cultured under aerobic and suboxic conditions by accurate mass and time tag approach, *Mol. Cell. Proteomics 5*, 714−725.
13. Adams, S. R., Campbell, R. E., Gross, L. A., Martin, B. R., Walkup, G. K., Yao, Y., Llopis, J., and Tsien, R. Y. (2002) New biarsenical ligands and tetracysteine motifs for protein labeling in vitro and in vivo: Synthesis and biological applications, *J. Am. Chem. Soc. 124*, 6063−6076.
14. Cao, H., Chen, B., Squier, T. C., and Mayer, M. U. (2006) CrAsH: A biarsenical multi-use affinity probe with low nonspecific fluorescence, *Chem. Commun.*, 2601−2603.
15. Myers, C. R., and Nealson, K. H. (1990) Respiration-linked proton translocation coupled to anaerobic reduction of manganese(IV) and iron(III) in *Shewanella putrefaciens* MR-1, *J. Bacteriol. 172*, 6232−6238.
16. Zachara, J. M., Fredrickson, J. K., Li, S., Kennedy, D. W., Smith, S. C., and Gassman, P. L. (1998) Bacterial reduction of crystalline Fe^{3+} oxides in single phase suspensions and subsurface materials, *Am. Mineral. 83*, 1426−1443.
17. Romine, M. F., Elias, D. A., Monroe, M. E., Auberry, K., Fang, R., Fredrickson, J. K., Anderson, G. A., Smith, R. D., and Lipton, M. S. (2004) Validation of *Shewanella oneidensis* MR-1 small proteins by AMT tag-based proteome analysis, *OMICS 8*, 239−254.
18. Tsai, P. S., Evans, J. E., Green, K. M., Sullivan, R. M., Schaumberg, D. A., Richards, S. M., Dana, M. R., and Sullivan, D. A. (2006) Proteomic analysis of human meibomian gland secretions, *Br. J. Ophthalmol. 90*, 372−377.
19. Sacksteder, C. A., Qian, W. J., Knyushko, T. V., Wang, H., Chin, M. H., Lacan, G., Melega, W. P., Camp, D. G., II, Smith, R. D., Smith, D. J., Squier, T. C., and Bigelow, D. J. (2006) Endogenously nitrated proteins in mouse brain: Links to neurodegenerative disease, *Biochemistry 45*, 8009−8022.
20. Haugland, R. P. (2005) in *Handbook of Fluorescent Probes and Research Chemicals*, 10th ed., Molecular Probes, Inc., Eugene, OR.
21. Shepherd, N., Dennis, P., and Bremer, H. (2001) Cytoplasmic RNA Polymerase in *Escherichia coli*, *J. Bacteriol. 183*, 2527−2534.
22. Arifuzzaman, M., Maeda, M., Itoh, A., Nishikata, K., Takita, C., Saito, R., Ara, T., Nakahigashi, K., Huang, H. C., Hirai, A., Tsuzuki, K., Nakamura, S., Altaf-Ul-Amin, M., Oshima, T., Baba, T., Yamamoto, N., Kawamura, T., Ioka-Nakamichi, T., Kitagawa, M., Tomita, M., Kanaya, S., Wada, C., and Mori, H. (2006) Large-scale identification of protein-protein interaction of *Escherichia coli* K-12, *Genome Res. 16*, 686−691.
23. Garcia, De La Torre, J., Huertas, M. L., and Carrasco, B. (2000) Calculation of hydrodynamic properties of globular proteins from their atomic-level structure, *Biophys. J. 78*, 719−730.
24. Travers, A. A., Debenham, P. G., and Pongs, O. (1980) Translation initiation factor 2 alters transcriptional selectivity of *Escherichia coli* ribonucleic acid polymerase, *Biochemistry 19*, 1651−1656.
25. Gralla, J. D. (2005) *Escherichia coli* ribosomal RNA transcription: Regulatory roles for ppGpp, NTPs, architectural proteins and a polymerase-binding protein, *Mol. Microbiol. 55*, 973−977.
26. Lund, P. A. (2001) Microbial molecular chaperones, *Adv. Microb. Physiol. 44*, 93−140.
27. Eisenmann, A., Schwarz, S., Prasch, S., Schweimer, K., and Rosch, P. (2005) The *E. coli* NusA carboxy-terminal domains are structurally similar and show specific RNAP- and λN interaction, *Protein Sci. 14*, 2018−2029.
28. Burillo, S., Luque, I., Fuentes, I., and Contreras, A. (2004) Interactions between the nitrogen signal transduction protein PII and N-acetyl glutamate kinase in organisms that perform oxygenic photosynthesis, *J. Bacteriol. 186*, 3346−3354.
29. Li, L., Jia, Y. H., and Pan, S. Q. (2002) *Agrobacterium flagellar* switch gene fliG is liquid inducible and important for virulence, *Can. J. Microbiol. 48*, 753−758.
30. Gupta, R., China, A., Manjunatha, U. H., Ponnanna, N. M., and Nagaraja, V. (2006) A complex of DNA gyrase and RNA polymerase fosters transcription in *Mycobacterium smegmatis*, *Biochem. Biophys. Res. Commun. 343*, 1141−1145.
31. Jormakka, M., Byrne, B., and Iwata, S. (2003) Formate dehydrogenase: A versatile enzyme in changing environments, *Curr. Opin. Struct. Biol. 13*, 418−423.
32. Shi, L., Chen, B., Wang, Z., Elias, D. A., Mayer, M. U., Gorby, Y. A., Ni, S., Lower, B. H., Kennedy, D. W., Wunschel, D. S., Mottaz, H. M., Marshall, M. J., Hill, E. A., Beliaev, A. S., Zachara, J. M., Fredrickson, J. K., and Squier, T. C. (2006) Isolation of a high-affinity functional protein complex between OmcA and MtrC: Two outer membrane decaheme c-type cytochromes of *Shewanella oneidensis* MR-1, *J. Bacteriol. 188*, 4705−4714.
33. Butland, G., Peregrin-Alvarez, J. M., Li, J., Yang, W., Yang, X., Canadien, V., Starostine, A., Richards, D., Beattie, B., Krogan, N., Davey, M., Parkinson, J., Greenblatt, J., and Emili, A. (2005) Interaction network containing conserved and essential protein complexes in *Escherichia coli*, *Nature 433*, 531−537.
34. Slauch, J. M., Russo, F. D., and Silhavy, T. J. (1991) Suppressor mutations in rpoA suggest that OmpR controls transcription by direct interaction with the α subunit of RNA polymerase, *J. Bacteriol. 173*, 7501−7510.
35. Gari, E., Bossi, L., and Figueroa-Bossi, N. (2001) Growth-dependent DNA breakage and cell death in a gyrase mutant of Salmonella, *Genetics 159*, 1405−1414.
36. Jovanovic, M., Lilic, M., Janjusevic, R., Jovanovic, G., and Savic, D. J. (1999) tRNA synthetase mutants of *Escherichia coli* K-12 are resistant to the gyrase inhibitor novobiocin, *J. Bacteriol. 181*, 2979−2983.

37. Baars, L., Ytterberg, A. J., Drew, D., Wagner, S., Thilo, C., van Wijk, K. J., and de Gier, J. W. (2006) Defining the role of the *Escherichia coli* chaperone SecB using comparative proteomics, *J. Biol. Chem. 281*, 10024−10034.
38. Saul, F. A., Arie, J. P., Vulliez-le Normand, B., Kahn, R., Betton, J. M., and Bentley, G. A. (2004) Structural and functional studies of FkpA from *Escherichia coli*, a cis/trans peptidyl-prolyl isomerase with chaperone activity, *J. Mol. Biol. 335*, 595−608.
39. Wong, T., Sosnick, T. R., and Pan, T. (2005) Mechanistic insights on the folding of a large ribozyme during transcription, *Biochemistry 44*, 7535−7542.
40. Mitsuzawa, H., Kimura, M., Kanda, E., and Ishihama, A. (2005) Glyceraldehyde-3-phosphate dehydrogenase and actin associate with RNA polymerase II and interact with its Rpb7 subunit, *FEBS Lett. 579*, 48−52.
41. Biran, D., Brot, N., Weissbach, H., and Ron, E. Z. (1995) Heat shock-dependent transcriptional activation of the metA gene of *Escherichia coli*, *J. Bacteriol. 177*, 1374−1379.
42. Kloft, N., and Forchhammer, K. (2005) Signal transduction protein PII phosphatase PphA is required for light-dependent control of nitrate utilization in *Synechocystis* sp. strain PCC 6803, *J. Bacteriol. 187*, 6683−6690.
43. Chilcott, G. S., and Hughes, K. T. (2000) Coupling of flagellar gene expression to flagellar assembly in *Salmonella enterica* serovar *typhimurium* and *Escherichia coli*, *Microbiol. Mol. Biol. Rev. 64*, 694−708.
44. Esberg, B., Leung, H. C., Tsui, H. C., Bjork, G. R., and Winkler, M. E. (1999) Identification of the miaB gene, involved in methylthiolation of isopentenylated A37 derivatives in the tRNA of *Salmonella typhimurium* and *Escherichia coli*, *J. Bacteriol. 181*, 7256−7265.
45. Mangroo, D., Limbach, P. A., McCloskey, J. A., and RajBhandary, U. L. (1995) An anticodon sequence mutant of *Escherichia coli* initiator tRNA: Possible importance of a newly acquired base modification next to the anticodon on its activity in initiation, *J. Bacteriol. 177*, 2858−2862.
46. Pierrel, F., Douki, T., Fontecave, M., and Atta, M. (2004) MiaB protein is a bifunctional radical-S-adenosylmethionine enzyme involved in thiolation and methylation of tRNA, *J. Biol. Chem. 279*, 47555−47563.
47. Mathu, S. G., Knudsen, C. R., van Duin, J., and Kraal, B. (2003) Isolation of Qβ polymerase complexes containing mutant species of elongation factor Tu, *J. Chromatogr., B: Anal. Technol. Biomed. Life Sci. 786*, 279−286.
48. Jafri, S., Urbanowski, M. L., and Stauffer, G. V. (1995) A mutation in the rpoA gene encoding the α subunit of RNA polymerase that affects metE-metR transcription in *Escherichia coli*, *J. Bacteriol. 177*, 524−529.
49. Nierman, W. C., and Chamberlin, M. J. (1980) Studies of RNA chain initiation by *Escherichia coli* RNA polymerase bound to T7 DNA. Direct analysis of the kinetics of RNA chain initiation at T7 promoter A2, *J. Biol. Chem. 255*, 1819−1823.
50. Jenal, U., and Hengge-Aronis, R. (2003) Regulation by proteolysis in bacterial cells, *Curr. Opin. Microbiol. 6*, 163−172.
51. Marcaida, M. J., DePristo, M. A., Chandran, V., Carpousis, A. J., and Luisi, B. F. (2006) The RNA degradosome: life in the fast lane of adaptive molecular evolution, *Trends Biochem. Sci. 31*, 359−365.
52. Sikder, D., Johnston, S. A., and Kodadek, T. (2006) Widespread, but Non-identical, Association of Proteasomal 19 and 20 S Proteins with Yeast Chromatin, *J. Biol. Chem. 281*, 27346−27355.
53. Gentry, D. R., and Cashel, M. (1996) Mutational analysis of the *Escherichia coli* spoT gene identifies distinct but overlapping regions involved in ppGpp synthesis and degradation, *Mol. Microbiol. 19*, 1373−1384.
54. Trchounian, A. (2004) *Escherichia coli* proton-translocating F0F1-ATP synthase and its association with solute secondary transporters and/or enzymes of anaerobic oxidation-reduction under fermentation, *Biochem. Biophys. Res. Commun. 315*, 1051−1057.

BI0621157